Path loss modeling for vehicle-to-vehicle communications

Kåredal, Johan; Czink, Nikolai; Paier, Alexander; Tufvesson, Fredrik; Molisch, Andreas

Published in:
IEEE Transactions on Vehicular Technology

DOI:
10.1109/TVT.2010.2094632

2011

performed by utilizing the broadcast nature of relay transmission, which provides an implicit feedback channel. Such a scheme minimizes the required feedback and reduces the additional overhead required at the relay for error detection, which results in an improvement in bandwidth efficiency. A strict performance upper bound for ICRIF with convolutional code is derived in a Rayleigh fading channel with AWGN. The analytical results presented in this paper have been verified through extensive simulation studies.

APPENDIX

With RCPC, a low-rate k/n code is periodically punctured with period P to obtain a family of codes with rate $P/(P+l)$, where l can be varied between 1 and $(N-1)P$ [11]. During the initial transmission, for every P information bits, $P+l_{init}$ bits are transmitted by SN. If DN asks for retransmission, then l_i redundant bits are transmitted by either SN or RN during the ith retransmission. The additional redundant bits are determined by the puncturing matrix.

In the viterbi algorithm (VA) decoding process, the decision of selecting a path is determined by the received path SNR. Only the nonpunctured bits contribute to the branch metrics. To calculate the average pair-wise error probability $P_d(q(\gamma_{SD;RD}))$, the average received path SNR needs to be computed.

The received SNR at DN for the bits transmitted from SN is $\gamma_{SD} = (|h_{SD}|^2\epsilon_s/N_0)$ and, from RN, is $\gamma_{RD} = (|h_{RD}|^2\epsilon_r/N_0)$. The received sequences are code combined before VA decoding. The average received path SNR can be computed based on the number of bits received with SNR γ_{SD} and γ_{RD}, respectively. Then, the average received path SNR at DN can be expressed as

$$\gamma_{SD;RD} = \beta_S \frac{|h_{SD}|^2\varepsilon_s}{N_0} + \beta_R \frac{|h_{RD}|^2\varepsilon_r}{N_0} \tag{11}$$

where β_S and β_R are the fraction of bits transmitted by SN and RN, respectively.

REFERENCES

[1] A. Sendonaris, E. Erkip, and B. Aazhang, "User cooperation diversity—Part I: System description," *IEEE Trans. Commun.*, vol. 51, no. 11, pp. 1927–1938, Nov. 2003.

[2] A. Sendonaris, E. Erkip, and B. Aazhang, "User cooperation diversity—Part II: Implementation aspects and performance analysis," *IEEE Trans. Commun.*, vol. 51, no. 11, pp. 1939–1948, Nov. 2003.

[3] J. N. Laneman, D. N. C. Tse, and G. W. Wornell, "Cooperative diversity in wireless networks: Efficient protocols and outage behavior," *IEEE Trans. Inf. Theory*, vol. 50, no. 12, pp. 3062–3080, Dec. 2004.

[4] T. E. Hunter and A. Nosratinia, "Diversity through coded cooperation," *IEEE Trans. Commun.*, vol. 5, no. 2, pp. 283–289, Feb. 2006.

[5] M. M. Feghhi and B. Abolhassani, "BER reduction through soft information relaying in incremental redundancy cooperative coded schemes," in *Proc. CNSR*, May 11–13, 2009, pp. 350–355.

[6] R. Liu, P. Spasojevic, and E. Soljanin, "Incremental redundancy cooperative coding for wireless networks: Cooperative diversity, coding, and transmission energy gains," *IEEE Trans. Inf. Theory*, vol. 54, no. 3, pp. 1207–1224, Mar. 2008.

[7] B. Zhao and M. C. Valenti, "Practical relay networks: A generalization of hybrid-ARQ," *IEEE J. Sel. Areas Commun.*, vol. 23, no. 1, pp. 7–18, Jan. 2005.

[8] A. J. Viterbi, "Convolutional codes and their performance in communication systems," *IEEE Trans. Commun. Technol.*, vol. COM-19, no. 5, pp. 751–772, Oct. 1971.

[9] J. G. Proakis, *Digital Communications*, 4th ed. New York: McGraw-Hill, 2001.

[10] W. C. Jakes, *Microwave Mobile Communications*, 2nd ed. New York: IEEE Press, 1993.

[11] J. Hagenauer, "Rate-compatible punctured convolutional codes (RCPC codes) and their applications," *IEEE Trans. Commun.*, vol. 36, no. 4, pp. 389–400, Apr. 1988.

[12] J. Ha, J. Kim, and S. W. McLaughlin, "Rate-compatible puncturing of low-density parity-check codes," *IEEE Trans. Inf. Theory*, vol. 50, no. 11, pp. 2824–2836, Nov. 2004.

Path Loss Modeling for Vehicle-to-Vehicle Communications

Johan Karedal, *Member, IEEE*, Nicolai Czink, *Member, IEEE*, Alexander Paier, *Student Member, IEEE*, Fredrik Tufvesson, *Senior Member, IEEE*, and Andreas F. Molisch, *Fellow, IEEE*

***Abstract*—Vehicle-to-vehicle (V2V) communications have received increasing attention lately, but there is a lack of reported results regarding important quantities such as path loss. This paper presents parameterized path loss models for V2V communications based on extensive sets of measurement data collected mainly under line-of-sight conditions in four different propagation environments: highway, rural, urban, and suburban. The results show that the path loss exponent is low for V2V communications, i.e., path loss slowly increases with increasing distance. We compare our results to those previously reported and find that, while they confirm some of the earlier work, there are also differences that motivate the need for further studies.**

***Index Terms*—Channel models, propagation constant, propagation losses, radio propagation, vehicles.**

I. INTRODUCTION

Vehicle-to-vehicle (V2V) communications offer numerous possible applications within, e.g., traffic safety enhancement, and has therefore received much attention in recent years. As in the development of any wireless system, knowledge of the propagation channel is vital for designers of V2V communication systems since its properties will ultimately dictate system performance. For those reasons, several V2V measurement campaigns have been conducted over the past few years, e.g., [1]–[9]. However, as recently pointed out in [10], there is still a lack of results regarding many important channel parameters.

Manuscript received May 10, 2010; revised July 9, 2010 and November 4, 2010; accepted November 4, 2010. Date of publication November 29, 2010; date of current version January 20, 2011. This work was supported in part by Kplus and Wiener Wissenschafts-, Forschungs- und Technologiefonds (WWTF) in the Forschungszentrum Telekommunikation Wien (FTW) projects I0 and I2 and in part by an Individual grants for the advancement of research leaders (INGVAR) grant of the Swedish Strategic Research Foundation (SSF), the SSF Center of Excellence for High-Speed Wireless Communications, and COST 2100. The review of this paper was coordinated by Dr. K. T. Wong.

J. Karedal and F. Tufvesson are with the Department of Electrical and Information Technology, Lund University, 221 00 Lund, Sweden (e-mail: Johan.Karedal@eit.lth.se; Fredrik.Tufvesson@eit.lth.se).

N. Czink is with the Forschungszentrum Telekommunikation Wien (FTW), 1220 Vienna, Austria (e-mail: czink@ftw.at).

A. Paier is with the Institut für Nachrichtentechnik und Hochfrequenztechnik, Technische Universität Wien, 1040 Vienna, Austria (e-mail: apaier@nt.tuwien.ac.at).

A. F. Molisch is with the Department of Electrical Engineering, University of Southern California, Los Angeles, CA 90089-0911 USA (e-mail: Andreas.Molisch@ieee.org).

Color versions of one or more of the figures in this paper are available online at http://ieeexplore.ieee.org.

Digital Object Identifier 10.1109/TVT.2010.2094632

Of particular interest is the *path loss*, which is the single most important quantity of any wireless channel. Since V2V communication systems are ad-hoc based and the transmitting nodes are highly dynamic, an understanding of path loss is particularly important for analysis of interference and scalability, i.e., situations when many nodes are densely packed in a small geographical area, e.g., congestion. In the measurements of path loss for V2V communications that exist in the literature, it has been found that, similar to other wireless systems, the path loss coefficient depends on the type of environment. Path loss results have been derived for *highway* [5], [8], [11],[1] *rural* [5], [8], *urban* [8], and *suburban* [3] environments. However, the number of existing measurements is too small to allow general statements about path loss behavior in those environments; path loss models in some environments are based on a single measurement campaign only. Hence, more measurement results are called for to reach statistically reliable conclusions.

This paper adds to the knowledge of path loss in V2V channels by presenting path loss models for four different environments: 1) highway; 2) rural; 3) urban; and 4) suburban scenarios. The results are derived from extensive V2V channel measurements conducted in Lund, Sweden, during 2007.

II. Methodology

A. V2V Channel Measurements

Propagation channel measurements were conducted using the RUSK LUND channel sounder, which performs multiple-input–multiple-output measurements based on the switched array principle. The equipment uses a multitone test signal of variable length to sound the channel and outputs samples of the complex time-variant channel transfer function $H(f,t)$. Each measurement was recorded during 9.984 s, where the transfer function was sampled every $\Delta t = 0.3072$ ms, thus providing a total of $N_t = 32\,500$ time samples. The measured frequency range was 5.2 ± 0.12 GHz, the test signal length was 3.2 μs, and the transmitter output power was 0.5 W. Both transmitter (Tx) and receiver (Rx) used a four-element patch antenna circular array with vertically polarized elements equispaced along the perimeter. Each antenna array was mounted on the platform of a small pickup truck overlooking the cab (the height was approximately 2.4 m), such that the antenna elements were oriented toward 45°, 135°, 225°, and 315° (where 0° is the forward direction of the vehicle), respectively. Both Tx and Rx also logged their respective Global Positioning System (GPS) coordinates during the measurements. More details on the measurement setup can be found in [11].

Four different traffic environments were measured. *Highway* measurements were performed on a 5.5-km-long two-lane highway strip cutting through the city of Lund. The total street width is approximately 23 m. The directions of travel are separated by a low (≈0.5 m) concrete wall, and the road side environment is characterized by fields, earth berms (constituting noise barriers), low-rise commercial buildings, road signs, and street lamps. Traffic density was low to medium. (The average traffic on the road strip was 33 000–38 000 cars/24 h during 2006.)

Rural measurements were taken on a one-lane 13-m-wide motorway just outside Lund, where the road-side environment contains mostly fields along with a few houses and road signs. There was almost no traffic during these measurements.

Urban measurements were conducted along a one-lane city street in Lund, where four-story buildings line the street on both sides. The street width is 9 m, with 2-m-wide sidewalks on each side. On one side, houses are in direct proximity of the sidewalk, whereas the other side has a line of trees in front of the buildings, occupying roughly 10 m of width. The roadside has a few open spaces in this scenario and contains many scattering objects such as signs, trees, street lamps, and parked cars. The street was fairly busy during measurements, with vehicles, pedestrians, and bicycles in motion.

Suburban measurements were performed on a one-lane street that is 9 m wide just outside the city center of Lund. The difference between this scenario and the urban one is that buildings are fewer and set back further from the curb (typically 10–40 m), buildings consist of a mixture of tall tenement buildings (10–12 stories) and low commercial buildings (e.g., a gas station and a car dealer), and there are several open areas (e.g., parking lots, small park areas, and a football pitch) in the vicinity. Traffic was similar to the urban scenario but had fewer pedestrians and bicyclists.

For each environment, measurements were made, with cars driving in the same direction (convoy) or in opposite directions. The measurements were mainly performed under conditions with line of sight (LOS) between Tx and Rx, although occasional obstruction of the LOS path did occur. No distinction between these cases is made in the following analysis, and we thus let the possibility of occasional shadowing be inherent in the subsequent models. During each ≈10-s measurement, Tx and Rx were driving at the same approximately constant speed, although this speed varied between different measurements. Twenty-one highway, 44 rural, 25 urban, and ten suburban measurements were conducted, equating a total of 52 million time samples of the channel transfer functions.

B. Path Loss Derivation

The path loss is determined from the measured transfer functions as follows: Denoting the transfer function between the Tx element n_T and the Rx element n_R sampled at frequency f_l and time t_k by $H[n_R, n_T, f_l, t_k]$, we derive the small-scale averaged channel gain at time t_k as

$$G_{\mathrm{ssa}}(t_k) = \frac{1}{MN_f} \sum_{n_R=1}^{N_R} \sum_{n_T=1}^{N_T} \sum_{l=1}^{N_f} \sum_{m=0}^{M-1} |H[n_R, n_T, f_l, t_k + m\Delta t]|^2 \tag{1}$$

for $t_k = 0, M\Delta t, \ldots, \lfloor N_t/M - 1 \rfloor M\Delta t$, where $N_R = N_T = 4$ are the number of transmit and receive antennas, respectively; $N_f = 769$ is the number of measured frequency points; $\Delta t = 0.3072$ ms is the sampling interval; $\lfloor \cdot \rfloor$ denotes the floor operation; and M is an integer that is selected for each measurement such that $M\Delta t$ is the time corresponding to an approximate movement of 20 (for convoy measurements) or ten wavelengths (for opposite direction measurements) of the Tx and Rx.[2] The integer M was chosen to ensure that the channel is sufficiently stationary during the averaging interval $M\Delta t$ [12]. The 3-dB beamwidth of the antenna elements, 85°, implies that summation over n_R and n_T effectively results in an aggregated antenna pattern of an approximately omnidirectional antenna (in the azimuth plane) with gain G_a. The variations of the aggregated antenna pattern over azimuth are less than 2 dB.

From $G_{\mathrm{ssa}}(t_k)$, the dB-valued path loss PL at time t_k is derived as

$$PL(t_k) = 2G_a - 10 \log_{10} G_{\mathrm{ssa}}(t_k) \tag{2}$$

[1] Reference [11] presents one particular result of those presented in this paper.

[2] No attempts to reduce the influence of noise was made since its influence was found to be minor on the path loss results in [11], which are a subset of the measurement data treated in this paper.

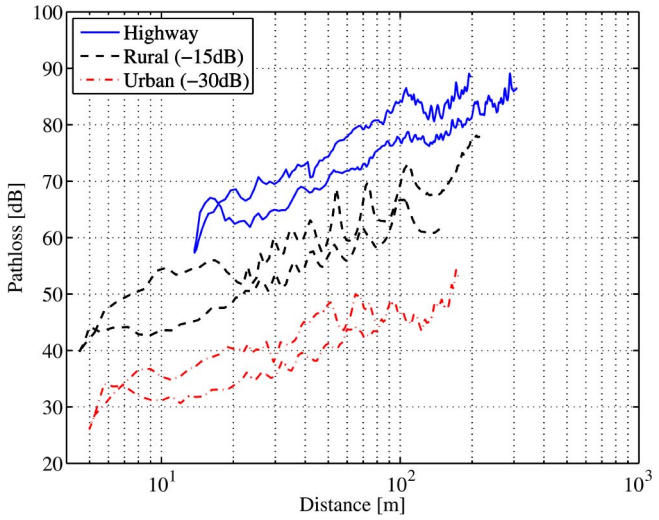

Fig. 1. Sample path loss for opposite direction measurements for highway, rural, and urban environments. For clarity, the rural results are plotted with a −15-dB vertical offset, whereas the urban results are plotted with a −30-dB vertical offset. Since the cars passed each other approximately in the middle of each measurement, there are two path loss values for (almost) every distance value. The lower curve corresponds to the time before the cars meet.

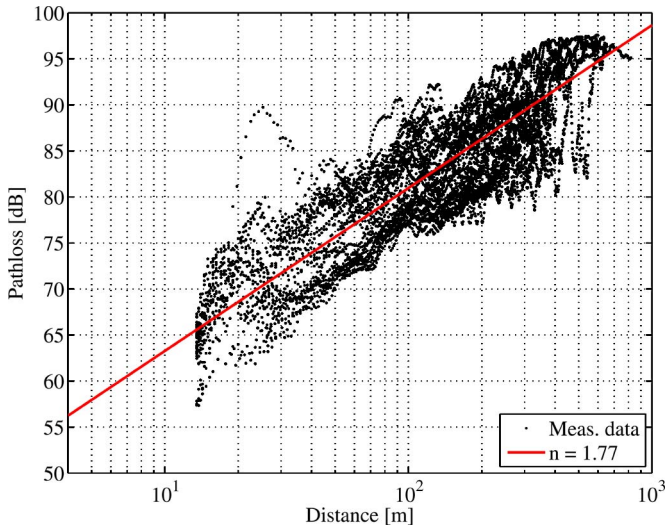

Fig. 2. Measured path loss for the highway environment and the best fit (in a least-square sense) to the deterministic part of (5). The large path loss values between $d = 20 - 30$ m are due to LOS obstruction in a particular measurement run.

where $G_a = 5.1$ dB is the average gain (over azimuth) of the aggregated antenna pattern at 5.2 GHz.[3] Finally, each time sample t_k is converted to the corresponding Tx-Rx distance d. Finding the GPS data too inaccurate for precise positioning, particularly at small distances and particularly in the urban scenario, we estimate d by determining the propagation delay τ_k of the first arriving multipath component, which is defined as the first component with a strength 5 dB above the noise floor.[4] Then, $d = \tau_k c$, where c is the speed of light. Finally, for measurements where the cars are driving in opposite directions, we adjust the estimated distances such that they match the true distance (lane-to-lane) at the point where the two cars meet.

III. Results and Modeling

A. General Observations

Examples of the resulting path loss when two cars drive toward each other, meet, and drive away from each other are shown for three different scenarios in Fig. 1.[5] Each curve corresponds to one 10-s measurement, and our first observation is that there is an offset between the path losses before and after the cars meet. (The upper part of each curve corresponds to the latter.) The offset is due to the *combined* gain of antennas and car being lower in the reverse direction; note that only the pure antenna influence is compensated for in (2). This reasoning is also confirmed by the path loss values from the convoy measurements, which, on average, are the approximate mean of the corresponding "forward" and "reverse" path loss.

Fig. 1 also shows that the distance dependence of path loss is different for different environments. The rural results show a structure similar to that of the well-known two-ray propagation model [13], which is reasonable since this environment provides few scatterers, i.e., the LOS path and its ground reflection are dominant. This is in contrast to the highway results, which rather indicate random variations around a distance-dependent decay. On the highway, the ground reflection is obstructed for long durations, usually by the concrete wall that separates the directions of travel or occasionally by other traffic. The urban results, on the other hand, can be interpreted as somewhere in between those of the highway and rural environments; there is a tendency of a two-ray structure, particularly before the cars meet, but obstruction of the ground reflection (e.g., from traffic) in combination with signal contributions from many other scattering objects creates path loss variations that are well described as random.

Figs. 2–5 show the extracted path loss from all measurements of each scenario. We note that the rural results are very consistent in terms of the highs and lows of the multiple measurements matching each other very well. An example of a situation with severe path loss can also be seen in Fig. 2; between $d = 20$ to 30 m, the path loss is some 20 dB larger than the average value due to an obstructed LOS path.

B. Modeling

For system simulations, modeling of the measured data is essential. As previously discussed, it is evident that there is a constant offset between the forward and reverse path loss that needs to be accounted for. Since neglecting this offset could lead to a too large variance of the modeled path loss at a given distance, we split the measurement data into ensembles of forward, reverse, and convoy data in the modeling process. For each environment, we extract separate model parameters for each ensemble and derive the final model parameters as the *average* over these ensembles. To account for the offset in the models, we introduce a correction term, which is added, subtracted, or neglected, depending on whether reverse, forward, or convoy path loss is considered.

[3]We thus approximate G_a as frequency independent, which is an assumption that is based on antenna calibration data (3-D antenna patterns) over 5.165–5.450 GHz; the variations of G_a are less than 0.4 dB over this range. However, since the aggregated antenna pattern in *azimuth* is not perfectly omnidirectional nor is it completely frequency invariant, it should be emphasized that the compensation for antenna impact in (2) is only approximate; full antenna compensation requires directional analysis of the propagation channel.

[4]To confirm the validity of this method, we also performed a visual inspection of the extracted propagation delay for each measurement.

[5]Due to practical difficulties, no measurements with cars traveling in opposite directions were made in the suburban environment; hence, no such sample result is shown.

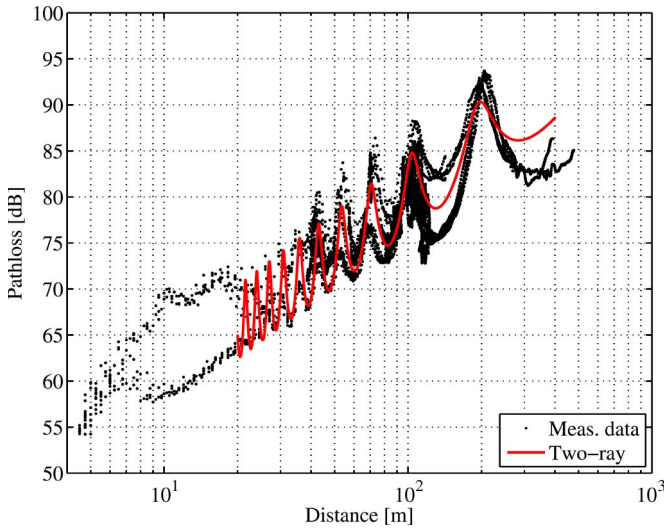

Fig. 3. Measured path loss for the rural environment and the best fit (in a least-square sense) to the deterministic part of (3).

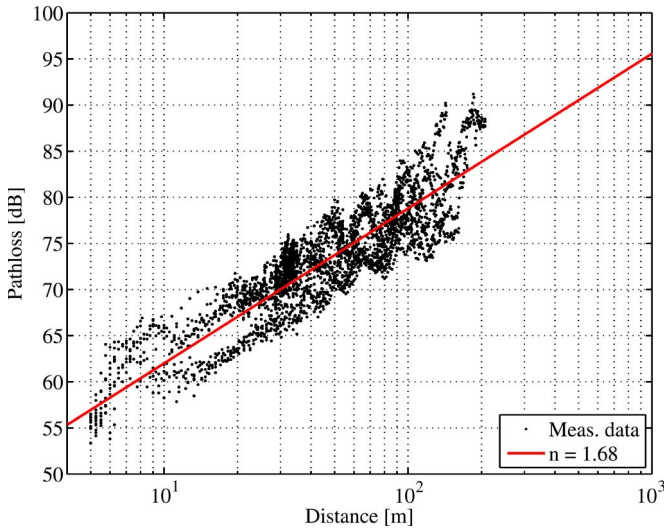

Fig. 4. Measured path loss for the urban environment and the best fit (in a least-square sense) to the deterministic part of (5).

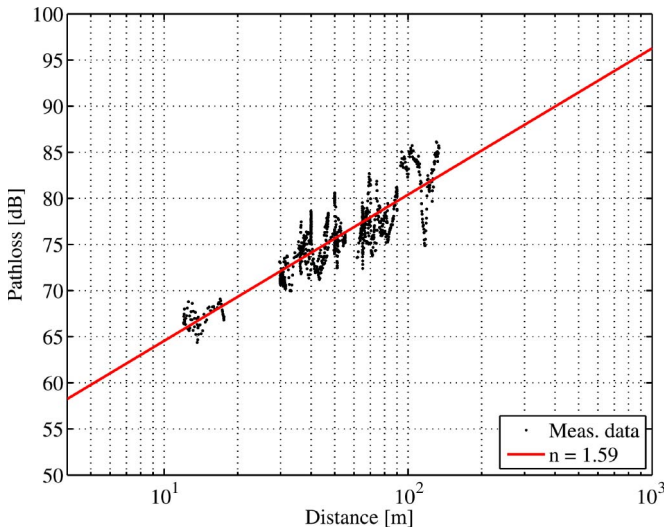

Fig. 5. Measured path loss for the suburban environment and the best fit (in a least-square sense) to the deterministic part of (5).

TABLE I
MODEL PARAMETERS; PL_0, G_{12}, PL_c, σ_1, AND σ_2 IN DECIBELS AND h IN METERS

Scenario	Power law		Two-ray model					
	PL_0	n	G_{12}	h	$\lvert\rho\rvert$	$\angle\rho$	$\sigma_{1,2}$	PL_c
Highway	63.3	1.77	–	–	–	–	3.1	3.3
Rural	–	–	7.3	2.53	0.44	$-131°$	2.6	2.3
Urban	62.0	1.68	–	–	–	–	1.7	1.5
Suburban	64.6	1.59	–	–	–	–	2.1	N/A

For the rural scenario, we model the path loss by a two-ray model [8], i.e., we let the path loss PL be given by

$$PL(d) = 20\log_{10}(4\pi f_c/c) - G_{12} + X_{\sigma_1} + \zeta PL_c - 20\log_{10}\left|\frac{\exp\{-jk_0 d\}}{d} + \rho\frac{\exp\{-jk_0\sqrt{d^2+4h^2}\}}{\sqrt{d^2+4h^2}}\right| \quad (3)$$

where d is the propagation (Tx-Rx) distance, h is the antenna height (which is equal on both link ends), ρ is the ground reflection coefficient, $k_0 = 2\pi f_c/c$ is the propagation number at the center frequency f_c, c is the speed of light, G_{12} is a constant, X_{σ_1} is a zero-mean normally distributed random variable with standard deviation σ_1, PL_c is a correction term that accounts for the offset between forward and reverse path loss, and ζ is defined as

$$\zeta = \begin{cases} 1, & \text{for reverse path loss} \\ -1, & \text{for forward path loss} \\ 0, & \text{for convoy path loss.} \end{cases} \quad (4)$$

Since the two-ray structure cannot be observed in the measurement data for small d, we limit the validity range of the model to $d \geq 20$ m. The best fit to the deterministic part of (3) (in a least-square sense) is shown along with the measurement data in Fig. 3.

Despite the tendency of a two-ray structure in the urban data, attempting to model these data with (3) fails to produce meaningful results. Instead, we apply the same model to the urban data as to the highway and suburban data: a classical power law. We thus let the path loss be given by

$$PL(d) = PL_0 + 10n\log_{10}(d/d_0) + X_{\sigma_2} + \zeta PL_c, \quad d > d_0 \quad (5)$$

where n is the path loss exponent, PL_0 is the path loss at a reference distance d_0, and X_{σ_2} is a zero-mean normally distributed random variable with standard deviation σ_2, whereas PL_c and ζ are as previously defined. Since there are few available samples for $d < 10$ m (none in the highway and suburban measurements), we let $d_0 = 10$ m and limit the validity range of the model to $d \geq 10$ m. PL_0 is thus the extrapolation of the path loss slope in the highway and suburban cases. The best fit to the deterministic part of (5) (in a least-square sense) are also shown in Figs. 2, 4 and 5. The extracted parameters for all models are summarized in Table I.

It is noteworthy that all extracted path loss exponents are lower than 2, which implies better-than-free-space propagation. Similar results have previously been reported for indoor propagation under LOS conditions mostly for ultrawideband channels [14], [15] but also for narrowband [16] and wideband channels [17], [18]. The common explanation is that there is, in addition to the LOS path, more energy available due to multipath propagation. As we will see later on, exponents lower than 2 have also been found in earlier work on V2V path loss modeling.

Since previous studies on V2V path loss have been based on smaller bandwidths (a 20-MHz bandwidth was used in [8], whereas

[3] and [5] were based on narrowband measurements), we investigate the bandwidth and frequency dependence of our model parameters before comparing them to earlier work. We do this by first separating each measured frequency response into 24 10-MHz bands and then applying the exact same data processing and parameter extraction as previously described for each subband. For each parameter and each scenario, we thus obtain an ensemble of 24 values.

From these results, we conclude that the difference between the mean of the 24 subband parameters and the corresponding parameter evaluated over 240 MHz is small; with the exception of σ_1 and σ_2, the relative difference is less than 1%. The standard deviations σ_1 and σ_2 increase by, on average, 0.2 dB when the bandwidth is reduced, which is reasonable since the bandwidth reduction implies less frequency averaging. We also find that the *absolute* path loss level, i.e., PL_0 and G_{12}, slightly increases with increasing frequency on average (over the four scenarios) by 1.6 dB. This increase is likely due to frequency dependence of the antenna patterns; since the gain at the boundary of the main lobe decreases with increasing frequency for the antenna elements we use, the gain in the forward direction of the vehicles will be reduced due to the way the antenna arrays were mounted. The frequency dependence of the remaining power law parameters is less consistent (over the different scenarios) and does not allow for any general conclusions; on average, there is a decrease in n and σ_1 over the measured band by 0.14 and 0.17, respectively. The remaining two-ray model parameters show effectively no dependence on frequency.

Our extracted parameters agree very well with those previously reported by Kunisch and Pamp [8], who used a power law model for highway $(n = 1.85, \sigma = 3.2)$ and urban $(n = 1.61, \sigma = 3.4)$ environments but found that a two-ray model was best suited for rural environments. A comparison of two-ray parameters is not as straightforward as path loss exponents, but it is noteworthy that the standard deviation (2.7 dB) is very close to ours. In addition, the reflection coefficient $(0.264 \angle -158^\circ)$ is reasonably similar, although it should be emphasized, as stated in [8], that this coefficient is not to be interpreted as that of the actual reflection process but rather as an *effective* measure. A similar reasoning applies to the extracted antenna height, but the estimated value compares very well to the actual antenna height. Specific details of the measurement setup and environments are scarce in [8], but it is mentioned that a portion of the rural data were collected when there was little to no other traffic, which is similar to our scenario, and that roof-mounted (1.6 m above ground) sleeve dipole antennas were used.

The measurements of Cheng *et al.* [3], [5] suggest that a breakpoint model is suitable to describe the path loss. Although this makes comparisons less straightforward, we can draw some conclusions by comparing their results before the breakpoint to our results. The highway result of [5] ($n = 1.9$ up to a breakpoint at 220 m) compares well with our estimate, but our extracted path loss exponent for the suburban case is lower than the two values reported in [3] ($n = 2$ and $n = 2.1$ up to a breakpoint at 100 m) and [5] ($n = 2.3$ up to a breakpoint at 226 m). It is also noteworthy that Cheng *et al.* [5] found a power law model to be suitable for rural scenarios. (The same authors, however, found support for a two-ray structure in [19], although no model parameters were derived.) These discrepancies are likely due to differences in the measurement setup or the selected propagation environments. However, an exact comparison of these is difficult. Whereas the street geometry of [5] is very similar to ours (8–10-m-wide single-lane streets, houses set back 10–12 m from the curb), there is no available information on building types, building density, traffic density, or presence of other likely scatterers. The antennas were roof mounted (at 1.51 and 1.93 m for Tx and Rx, respectively) and had the same gain in both forward and reverse directions.

IV. Summary

We have presented path loss results and models for four different environments, where V2V communication systems are expected to be useful; these models can be applied to system design and simulation. We have found that the estimated path loss exponents are low for all environments, which indicates that designs that are robust to interference from other users should be considered for V2V systems. Our results have confirmed those previously reported by Kunisch and Pamp [8] for highway, urban, and rural environments, both in terms of the most suitable propagation models and their parameters. There are, however, some discrepancies between our results and those by Cheng *et al.* [3], [5], particularly for rural and suburban scenarios. These are likely explained by differences in the propagation environments, which motivates the need for further studies of path loss for V2V systems.

Acknowledgment

The authors would like to thank Dr. C. Dumard, Dr. H. Hofstetter, Dr. T. Zemen, and Dr. C. F. Mecklenbräuker for their assistance during the measurement campaign.

References

[1] J. Maurer, T. Fügen, and W. Wiesbeck, "Narrow-band measurement and analysis of the inter-vehicle transmission channel at 5.2 GHz," in *Proc. IEEE Veh. Technol. Conf.—Spring*, 2002, vol. 3, pp. 1274–1278.

[2] A. Paier, J. Karedal, N. Czink, H. Hofstetter, C. Dumard, T. Zemen, F. Tufvesson, A. F. Molisch, and C. F. Mecklenbräuker, "Car-to-car radio channel measurements at 5 GHz: Path loss, power-delay profile, and delay-Doppler spectrum," in *Proc. Int. Symp. Wireless Commun. Syst.*, 2007, pp. 224–228.

[3] L. Cheng, B. Henty, D. Stancil, F. Bai, and P. Mudalige, "Mobile vehicle-to-vehicle narrow-band channel measurement and characterization of the 5.9 GHz dedicated short range communication (DSRC) frequency band," *IEEE J. Sel. Areas Commun.*, vol. 25, no. 8, pp. 1501–1516, Oct. 2007.

[4] L. Cheng, B. Henty, R. Cooper, D. D. Stancil, and F. Bai, "Multi-path propagation measurements for vehicular networks at 5.9 GHz," in *Proc. IEEE Wireless Commun. Netw. Conf.*, Apr. 2008, pp. 1239–1244.

[5] L. Cheng, B. E. Henty, F. Bai, and D. D. Stancil, "Highway and rural propagation channel modeling for vehicle-to-vehicle communications at 5.9 GHz," in *Proc. IEEE Antennas Propag. Soc. Int. Symp.*, Jul. 2008, pp. 1–4.

[6] I. Sen and D. W. Matolak, "Vehicle-vehicle channel models for the 5-GHz band," *IEEE Trans. Intell. Transp. Syst.*, vol. 9, no. 2, pp. 235–245, Jun. 2008.

[7] I. Tan, W. Tang, K. Laberteaux, and A. Bahai, "Measurement and analysis of wireless channel impairments in DSRC vehicular communications," in *Proc. IEEE Int. Conf. Commun.*, 2008, pp. 4882–4888.

[8] J. Kunisch and J. Pamp, "Wideband car-to-car radio channel measurements and model at 5.9 GHz," in *Proc. IEEE Veh. Technol. Conf.—Fall*, Sep. 2008, pp. 1–5.

[9] O. Renaudin, V. M. Kolmonen, P. Vainikainen, and C. Oestges, "Wide-band MIMO car-to-car radio channel measurements at 5.3 GHz," in *Proc. IEEE Veh. Technol. Conf.—Fall*, Sep. 2008, pp. 1–5.

[10] A. F. Molisch, F. Tufvesson, J. Karedal, and C. Mecklenbräuker, "A survey on vehicle-to-vehicle propagation channels," *IEEE Wireless Commun.*, vol. 16, no. 6, pp. 12–22, Dec. 2009.

[11] A. Paier, J. Karedal, N. Czink, C. Dumard, T. Zemen, F. Tufvesson, A. Molisch, and C. Mecklenbräuker, "Characterization of vehicle-to-vehicle radio channels from measurements at 5.2 GHz," *Wireless Pers. Commun.*, vol. 50, no. 1, pp. 19–32, Jul. 2009.

[12] L. Bernadó, T. Zemen, A. Paier, J. Karedal, and B. H. Fleury, "Parametrization of the local scattering function estimator for vehicular-to-vehicular channels," in *Proc. IEEE Veh. Technol. Conf.—Fall*, 2009, pp. 1–5.

[13] A. F. Molisch, *Wireless Communications*. Chichester, U.K.: Wiley, 2005.

[14] S. S. Ghassemzadeh, R. Jana, C. W. Rice, W. Turin, and V. Tarokh, "A statistical path loss model for in-home UWB channels," in *IEEE Conf. Ultra Wideband Syst. Technol. Dig. Tech. Papers*, 2002, pp. 59–64.

[15] J. A. Dabin, N. Ni, A. M. Haimovich, E. Niver, and H. Grebel, "The effects of antenna directivity on path loss and multipath propagation in UWB indoor wireless channels," in *IEEE Conf. Ultra Wideband Syst. Technol. Dig. Tech. Papers*, Reston, VA, Nov. 2003, pp. 305–309.
[16] J. Medbo and J.-E. Berg, "Simple and accurate path loss modeling at 5 GHz in indoor environments with corridors," in *Proc. IEEE Veh. Technol. Conf.—Fall*, Sep. 2000, vol. 1, pp. 30–36.
[17] A. A. M. Saleh and R. A. Valenzuela, "A statistical model for indoor multipath propagation," *IEEE J. Sel. Areas Commun.*, vol. SAC-5, no. 2, pp. 128–137, Feb. 1987.
[18] T. S. Rappaport and D. A. Hawbaker, "Wide-band microwave propagation parameters using circular and linear polarized antennas for indoor wireless channels," *IEEE Trans. Commun.*, vol. 40, no. 2, pp. 240–245, Feb. 1992.
[19] L. Cheng, B. E. Henty, F. Bai, and D. D. Stancil, "Doppler spread and coherence time of rural and highway vehicle-to-vehicle channels at 5.9 GHz," in *Proc. IEEE Global Commun. Conf.*, Nov. 2008, pp. 1–6.

Performance Analysis of QRD-Based Cyclically Prefixed Single-Carrier Transmissions With Opportunistic Scheduling

Kyeong Jin Kim, *Member, IEEE*, and
Theodoros A. Tsiftsis, *Senior Member, IEEE*

***Abstract*—The maximum average achievable rate and the outage probability of the opportunistic scheduling over the cyclically prefixed (CP) single-carrier (SC) downlink transmissions are analyzed. In the user terminal, the QR-decomposition (QRD)-based receiver is employed to maintain the multipath diversity gain. Based on the proposed receiver, closed-form expressions for the maximum average achievable rate and the outage probability can be derived using the property of the circulant matrix. In addition, the outage diversity gain is obtained at high average signal-to-noise ratio (SNR). Simulations verified the derived analysis.**

***Index Terms*—Average rate, cyclically prefixed (CP) single-carrier (SC) transmission, opportunistic scheduling, outage probability, QR decomposition (QRD)-based receiver.**

I. Introduction

Cyclically prefixed (CP) single-carrier (SC) systems [1]–[3] have been proposed in very high-speed wireless networks for short-range broadband applications to reduce the peak-to-average power ratio and power back-off requirement. With the help of this SC transmission, wireless high-definition multimedia interface, gaming interfaces, and high-speed backhaul and content distribution services may be possible applications. Targeting multiple gigabit-per-second throughputs, the next generation of wireless personal area network is already proposed in [4]–[6].

To fully support multiple users in the downlink, opportunistic scheduling is proposed in the orthogonal frequency-division multiple-access system [7]. With an exactly known channel state information (CSI) across all active users, an opportunistic scheduling is able to maximize the sum of the transmission data rate [8] since different users experience different channel environments at a given subcarrier. Moreover, the throughput improvement can be maintained by virtue of the multiuser diversity gain obtained from the opportunistic user selection mechanism [9], [10]. The frame error rate using the frequency-domain equalization (FDE) is also used in computing the spectral efficiency. Since SC FDE cannot exploit multipath diversity without applying channel coding [11], the QR decomposition (QRD)-based receiver is employed [12], [13]. Directly applying the QRD to the circulant channel matrix in the time domain, the multipath diversity gain can be maintained. This is the advantage of the QRD-based receiver in the CP SC system, compared with the FDE-based receivers [1]–[3]. Moreover, from the derived outage analysis, the number of channel taps is also shown to be an important factor in determining the outage diversity gain and maintaining the improved achievable average rate of the CP SC transmission. Individual QRD-based receivers and opportunistic scheduling are well known. The contribution of this paper is that it combines these techniques in the CP SC systems to improve its overall achievable rate while maintaining multiuser diversity gain. Furthermore, we provide closed-form expressions to verify its performances in terms of the maximum average achievable rate and the outage probability. In addition, the outage diversity gain is obtained at a high average signal-to-noise ratio (SNR). With the help of the QRD-based receiver, we are able to derive closed-form expressions for the preceding performance metrics without using the FDE [1], [2]. At specific scenarios, the derivations are verified from Monte Carlo simulations.

The rest of this paper is organized as follows: In Section II, the system and application of the QRD on the channel matrix are introduced. The throughput analysis of the opportunistic user selection and outage analysis are presented in Sections III and IV, respectively. Performance results are presented in Section V, and some concluding remarks are drawn in Section VI.

II. System and Channel Model

In this paper, we consider CP SC transmission where one base station (BS) will schedule to transmit data to K distinct user equipment (UE) sharing physical resources. Let the transmission symbol block after applying Gray mapping be denoted by $\boldsymbol{d}(n) \in \mathbb{C}^N$ with its kth element $d_k(n)$. One transmission block consists of N symbols, i.e., $\boldsymbol{d}(n) = [d_1(n), \ldots, d_N(n)]^T$. A CP of N_g symbols is employed to the front of the transmission block to prevent intersymbol interference. The instantaneous channel between the BS and the kth UE is denoted by $\boldsymbol{h}^k(n) \triangleq [h_0^k(n), \ldots, h_{N_f-1}^k(n)]^T$, with N_f being the channel order. The length of the CP is assumed to comprise the maximum path delay, i.e., $N_f \leq N_g$. The BS broadcasts its transmission symbol block to all UEs over the corresponding channels between the BS and all terminals. The received vector signal at the kth UE after eliminating CP becomes

$$\tilde{\boldsymbol{y}}^k(n) = \boldsymbol{H}_{\mathrm{cir}}^k(n)\boldsymbol{d}(n) + \tilde{\boldsymbol{z}}^k(n) \tag{1}$$

where $\boldsymbol{H}_{\mathrm{cir}}^k(n) \in \mathbb{C}^{N\times N}$ is a time-variant circulant matrix such that $(\boldsymbol{H}_{\mathrm{cir}}^k(n))(j,l) = h_{\langle j-l\rangle_N}^k(n)$, where $\langle\cdot\rangle_N$ denotes modulo-N operation, and $\tilde{\boldsymbol{z}}^k(n)$ is the noise vector one-sided power spectral density N_0, which can be modeled as a circularly symmetric complex Gaussian random variable with zero mean and variance σ_n^2, i.e., $\tilde{\boldsymbol{z}}^k(n) \sim \mathcal{CN}(\boldsymbol{0}, \sigma_n^2 \boldsymbol{I}_{N\times N})$, where $\boldsymbol{I}_{N\times N}$ is the $N \times N$ identity matrix. One transmission consists of P blocks of length-N symbols. We assume that the channel is static over $P(N + N_g)$ symbols, but it varies between transmissions.

Manuscript received February 9, 2010; revised April 18, 2010; accepted June 10, 2010. Date of publication June 28, 2010; date of current version January 20, 2011. The review of this paper was coordinated by Prof. J. Wu.

K. J. Kim is with UWB Wireless Communications Research Center, Inha University, Incheon, Korea (e-mail: kyeong.j.kim@hotmail.com).

T. A. Tsiftsis is with the Department of Electrical Engineering, Technological Educational Institute of Lamia, 35100 Lamia, Greece (e-mail: tsiftsis@teilam.gr).

Color versions of one or more of the figures in this paper are available online at http://ieeexplore.ieee.org.

Digital Object Identifier 10.1109/TVT.2010.2054122